

Power flow calculation for a distribution system with multi-port PETs: an improved AC-DC decoupling iterative method

Hang Yin¹, Qiang Li², Youbo Liu¹, Xianglong Liu¹, Yue Xiang^{1,3}, Junyong Liu¹

1. School of Electrical Engineering, Sichuan University, Chengdu, Sichuan Province, P.R. China

2. State Grid Jiangsu Electric Power Research Institute, Nanjing, Jiangsu Province, P.R. China

3. Department of Electrical and Electronic Engineering, Imperial College London, London SW7 2AZ, U.K.



Scan for more details

Abstract: Recently, power electronic transformers (PETs) have received widespread attention owing to their flexible networking, diverse operating modes, and abundant control objects. In this study, we established a steady-state model of PETs and applied it to the power flow calculation of AC–DC hybrid systems with PETs, considering the topology, power balance, loss, and control characteristics of multi-port PETs. To address new problems caused by the introduction of the PET port and control equations to the power flow calculation, this study proposes an iterative method of AC–DC mixed power flow decoupling based on step optimization, which can achieve AC–DC decoupling and effectively improve convergence. The results show that the proposed algorithm improves the iterative method and overcomes the over-correction and initial value sensitivity problems of conventional iterative algorithms.

Keywords: Power electronic transformers, AC–DC distribution systems, AC–DC mixed power flow algorithm.

1 Introduction

Power electronic transformers (PETs) can achieve independent, fast, and accurate control of the transmission power and voltage of each port [1]–[4]. Currently, research on PETs has focused mainly on the design of their internal structure, assembly-level simulation, and controller design.

A topology, as well as the associated modeling analysis and control scheme of multi-port PETs with multi-winding medium-frequency transformer isolation, was proposed in the study of [5]. In the study of [6], the unbalanced-load correction capability of two typical PET topologies were analyzed and compared.

However, because the topology, operating characteristics, and control methods of PETs do not have a unified standard, relatively few studies were conducted on the operational control of the steady-state model of PETs. A novel method was proposed for steady-state and dynamic load flow calculations, as well as a method for the automatic participation of a meshed HVDC grid in load frequency control causing load flows and a decentralized DC voltage control [7]. A steady-state voltage source converter multi-

Received: 12 April 2020/ Accepted: 2 July 2020/ Published: 25 August 2020

✉ Youbo Liu
liuyoubo@scu.edu.cn

Hang Yin
suiyue0828@163.com

Qiang Li
35830342@qq.com

Xianglong Liu
1044881755@qq.com

Yue Xiang
xiang@scu.edu.cn

Junyong Liu
liujy@scu.edu.cn

terminal direct current (VSC-MTDC) model for power flow programs was proposed by [8], allowing the simulation of multiple AC grids interconnected by multiple DC grids. Reference [9] proposed an improved analytical model, derived from the bisection algorithm and superposition principle to investigate the steady-state performance of droop-controlled VSC-MTDC systems under the conditions of converter outage and converter overload. Further, Reference [10] proposed detailed steady-state and transient stability investigative models of PETs.

At present, AC-DC power flow algorithms are categorized into two types: the unified iterative method and the alternating iterative method [11]-[14]. The advantages and disadvantages of the two types of algorithms have been compared in detail in the study of [15]. The alternating iteration method is more computationally efficient than the unified iteration method. Moreover, owing to the decoupling iteration of the DC system and the AC system, the systems can be solved using different algorithms, so the alternating iteration method exhibits good scalability and portability. The power flow calculation of the AC-DC hybrid distribution network has two problems:

1) The converter and DC system equipment in AC-DC power distribution systems has many types, and their power characteristics and control methods are complex; hence, system modeling is more difficult than that of a traditional distribution network [16]-[18]. Reference [19] proposed a decentralized optimal power flow model for running autonomous AC-DC hybrid microgrids, which considered the multipoint coordinated control strategy of PETs. Reference [20] categorized distributed power and energy storage into two, namely, controllable and uncontrollable, and divided the controllable sources into AC and DC sources. However, this method is not equivalent to the droop control grid connection point. Referring to the ZIP load model of the AC distribution network, [21] categorized the DC load into three, namely, constant resistance, constant current, and constant power, and performed a mixed power flow calculation. To ensure the accuracy the DC transformer model, [22] added the DC voltage control equation of the primary and secondary sides on the basis of the study of [21].

2) The AC-DC hybrid distribution network contains many DC links, and the traditional algorithm is difficult to ensure effective convergence in the case of large-scale multi-DC feeding; thus, traditional AC-DC hybrid power flow algorithms or models should be improved [23]-[25]. Reference [26] proposed that the DC system be optimized first, only to iterate the AC system and to verify the DC variables after the AC power flow converges. This method avoids the problem of DC divergence due to the oscillation

of DC variables in the alternating iteration process. Reference [27] suggested that large-scale DC systems are equipped with multiple DC relaxation nodes to achieve power flow convergence. According to [28], in a grid with many DC links, the dynamic model of the converter should be used to establish a quasi-steady-state power flow calculation model for the AC-DC hybrid system.

In this study, first, considering the topology, power balance, loss, and control characteristics of multi-port PETs, we established a steady-state model of power balance, internal coupling, losses, and control methods of the PET ports. Then, the proposed steady-state model was used in the power flow calculation of the AC-DC hybrid system with PETs. Owing to the complexity of the PET port equations and the associated governing equations, we proposed a decoupling iterative algorithm for AC-DC mixed power flow based on step size optimization. Finally, an example is provided to verify the effectiveness of the proposed algorithm, which can adapt to the coupling between the switching of the PET control modes and the power balance of multi-port PET ports.

2 Characteristics of power distribution network system with high proportion of renewable energy

Owing to the increasing penetration of distributed renewable energy in the power distribution network and the advance of the power electronic processes of the distribution system, the components of the distribution system and the structure and interaction of the participants have changed profoundly.

At the system level (Fig. 1), distributed wind power and photovoltaics are connected to the distribution network on a large scale. Meanwhile, electric vehicles and energy storage can also be regarded as a flexible power supply, which elevates uncertainty to the source end of the grid. The form of the network is manifested by the diversification of the system's networking mode, and the manner of the interactive coupling of power between AC, DC, and microgrids also differ, mainly determined by the function of power electronic power conversion devices, the abundance of network forms and multi-form, and multi-functional power electronic power conversion devices, which make the operational mode of AC-DC hybrid systems more complicated [29].

At the load side, many source loads with active response capabilities and two-way interaction capabilities exist, which requires users to participate in energy management. It also introduces new uncertainties to the load side. At

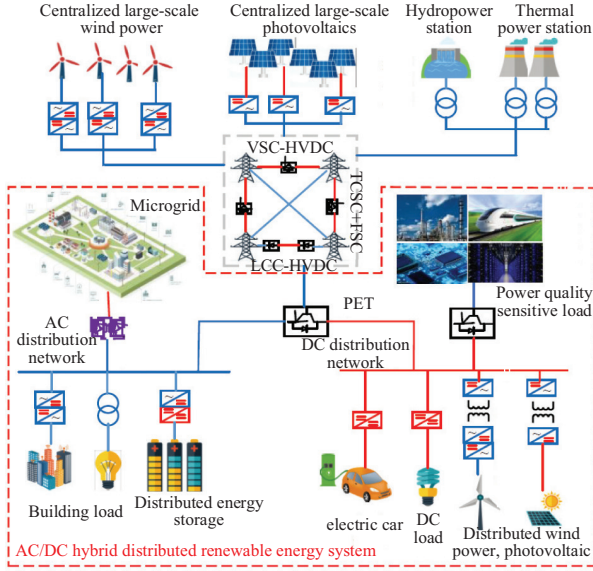


Fig. 1 Structure and elements of the future power system

the device level, distributed power supply grid connection devices, flexible interconnection devices, power quality management equipment, DC system protection, isolation devices, and integrated power distribution terminal units all become more intelligent and modularized, boasting higher power density and higher energy density. The distribution network has experienced progress too, from free power flow to controllable power flow, which supports the system-level intelligent application of each link of the source-network-load-storage and secondary system.

The future power system of Fig. 1 has the following four characteristics:

1) Improvement in the integration of the power control and communication control units has created the basic conditions for large-scale coordinated control of equipment.

2) Modular multilevel, pulse width modulation, and other power conversion technologies have complementary advantages in different application scenarios, thereby improving the energy efficiency of the power system.

3) Power conversion units can be flexibly combined, with multiple cascades, multiple ports, multiple flow directions, and multiple forms.

4) There are many fully controlled devices in the future power system, which has a high degree of dispersion and nonlinearity.

3 Steady-state model of multi-port PETs

3.1 Power flow calculation model of multi-port PETs

Fig. 2 shows the generalized steady-state equivalent model of multi-port PETs. The PET model can be described by equations (1)–(8), the AC port can be described by

equations (1)–(4), and the DC port can be described by equations (5)–(8). Here, superscript H represents the network side, including the AC network node at the far end of the AC–DC converter (node 2 shown in Fig. 2) and the DC node (node 4 shown in Fig. 2) connected to the secondary side of the DC–DC converter. Meanwhile, superscript D represents the PET port side, including the near-end AC node of the AC–DC converter (node 1 shown in Fig. 2) or the primary port node of the DC–DC converter (node 2 shown in Fig. 2).

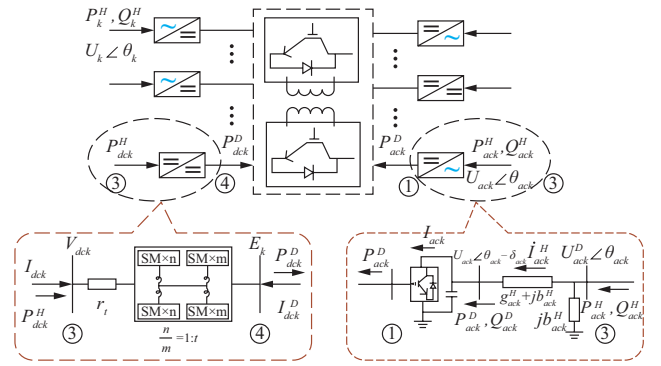


Fig. 2 Generalized steady-state model of the multi-port PET

$$P_{ack}^H = g_{ack}^H (U_{ack}^H)^2 - (g_{ack}^H \cos \delta_{ack} + b_{ack}^H \sin \delta_{ack}) U_{ack}^H U_{ack}^D \quad (1)$$

$$Q_{ack}^H = -(b_{ack}^H + b_{ack}^H) (U_{ack}^H)^2 + (b_{ack}^H \cos \delta_{ack} - g_{ack}^H \sin \delta_{ack}) U_{ack}^H U_{ack}^D \quad (2)$$

$$P_{ack}^D = E_{ack} I_{ack} = -g_{ack}^H (U_{ack}^D)^2 + (g_{ack}^H \cos \delta_{ack} - b_{ack}^H \sin \delta_{ack}) U_{ack}^H U_{ack}^D \quad (3)$$

$$E_{ack} = w_{ack} U_{ack}^D \quad (4)$$

$$E_{dck} / t + r_t I_{dck} = U_{dck}^H \quad (5)$$

$$P_{dck}^D = -E_{dck} I_{dck}^D = E_{dck} I_{dck} / t \quad (6)$$

$$P_{dck}^H = 2U_{dck}^H \sum_{i \in N} Y_{dcj} (U_{dck}^H - U_{dcj}^H) + U_{dck}^H I_{dck} \quad (7)$$

$$\sum_{ack \in \Phi} P_{ack}^D + \sum_{dck \in \Psi} P_{dck}^D = \Delta P_{loss}^{PET} \quad (8)$$

At the AC port side, P_{ack}^H and Q_{ack}^H represent the injected active and reactive power at the AC port of the PET (the subscript *ack* represents the AC port number), U_{ack}^D represents the voltage amplitude of the AC node on the port side of the AC port, and U_{ack}^H represents the voltage amplitude of the AC node on the network side of the port. Further, δ_{ack} indicates the phase angle of the node voltage of the AC port converter on the port side (which lags the

voltage of the node on the network side), $g_{ack}^H + jb_{ack}^H$ is the equivalent admittance of the power loss, and jb_{ack}^H denotes the AC port equivalent susceptance of parallel reactive power loss. Moreover, E_{ack} represents the DC side voltage of the AC–DC converter of the AC port, I_{ack} is the DC side current of the AC–DC converter, and P_{ack}^D represents the exchange power between the AC port and the PET.

At the DC port side, U_{dck}^H represents the DC voltage on the secondary side of the DC port (the subscript dck represents the DC port number), P_{dck}^H indicates the power injected into the DC port from the network connected to the DC port, I_{dck} represents the DC port current on the secondary side of the DC–DC converter, P_{dck}^D represents the exchange power between the primary side of the DC port converter and the power electronic transformer, E_{dck} represents the DC voltage on the primary side of the DC port converter, I_{dck}^D represents the DC current on the primary side of the DC port converter, and ΔP_{loss}^{PET} represents the comprehensive loss of the PET.

3.2 Loss equation of multi-port power electronic transformer

The total loss of the multi-port PETs can be equivalent to the sum of the AC port loss and the DC port loss. The loss equations of the two types of ports can be expressed in the form of quadratic equations.

$$\Delta P_{loss}^{PET} = \Delta P_{ack}^{loss} + \Delta P_{dck}^{loss} \quad (9)$$

$$\Delta P_{ack}^{loss} = a_{1k} I_{ack}^2 + a_{2k} I_{ack} + a_{3k} \quad (10)$$

$$\Delta P_{dck}^{loss} = a_{1k} I_{dck}^2 + a_{2k} I_{dck} + a_{3k} \quad (11)$$

$$I_{ack} = \frac{\sqrt{(P_{ack}^H)^2 + (Q_{ack}^H)^2}}{U_{ack}^H} \quad (12)$$

$$I_{dck} = \frac{P_{dck}^H}{U_{dck}^H} \quad (13)$$

Here, ΔP_{ack}^{loss} represents the comprehensive loss of the AC port, ΔP_{dck}^{loss} is the comprehensive loss of the DC port, and a_{3k} denotes the fixed loss coefficient, which represents the high-frequency core loss of the PET. Further, a_{2k} is the linear loss coefficient, which represents the switching loss in the PET; a_{1k} is the high-order loss coefficient, indicating the conduction loss of the switching device and the coil loss of the high-frequency transformer; I_{dck} represents the injected current at the DC port; and I_{ack} represents the injected current at the AC port.

3.3 Control equation of multi-port PETs

Each port of the PET can have a different control

mode, which can independently control the voltage of their connected nodes and the transmission power of the port. Owing to the current decoupling control of the port converter, active power, and reactive power can be controlled independently. Table 1 present the operating mode of the PET.

Table 1 Operating mode of the PET

Mode	Active power control	Reactive power control	
AC port	s1	P_{ack}^H constant	Q_{ack}^H constant
	s2	/	U_{ack}^H constant
	s3	/	Q_{ack}^H constant
	s4	P_{ack}^H constant	U_{ack}^H constant
DC port	d1	U_{dck}^H constant	/
	d2	P_{dck}^H constant	/
	d3	$P_{dck}^H - U_{dck}^H$ Sag	/

Table 2 present the control equations corresponding to the control modes in Table 1.

Table 2 The operating mode of the PET

Control mode	Control equations
P_k^H constant	$P_k^H - P_{k,set}^H = 0$
Q_k^H constant	$Q_k^H - Q_{k,set}^H = 0$
U_k^H constant	$U_k^H - U_{k,set}^H = 0$
U_{dck}^H constant	$U_{dck}^H - U_{dck,set}^H = 0$
P_{dck}^H constant	$P_{dck}^H - P_{dck,set}^H = 0$
$P_{dck}^H - U_{dck}^H$ Sag	$P_{dck}^H - P_{dck,set}^H = K(U_{dck}^H - U_{dck,set}^H)$

In the table, the subscript *set* indicates the value of the control variable of the port, and K represents the droop control coefficient. When the network contains multiple PETs, the master-slave control and the droop control are among the control strategy adopted by the DC port. In the master-slave control mode, a PET DC port must be controlled in a fixed DC voltage mode to maintain the DC node voltage. Meanwhile, the droop control can realize the automatic coordination of the DC voltage setting value and the automatic distribution of power between each DC port, by limiting the slope relationship between the DC power of each PET DC port and the DC voltage.

The AC port of the PET can independently control the active power and reactive power without being restricted by the power balance equation. Therefore, to achieve a unified

expression of the control equation as equations (14)–(16), the active and reactive control coefficients can be introduced for the state quantities under different control strategies.

$$\Delta P_{ack}^H = \eta_p (P_{ack}^H - P_{ack,set}^H) \quad (14)$$

$$\Delta Q_{ack}^H = \eta_Q (Q_{ack}^H - Q_{ack,set}^H) + (1 - \eta_Q)(U_{ack}^H - U_{ack,set}^H) \quad (15)$$

$$\Delta P_{dck}^H = \eta_p (P_{dck}^H - P_{dck,set}^H) + \eta_Q (1 - \eta_p)(U_{dck}^H - U_{dck,set}^H) + (1 - \eta_p)[P_{dck}^H - K(U_{dck}^H - U_{dck,set}^H)] \quad (16)$$

Here, η_p and η_Q represent the active power adjustment coefficient and reactive power adjustment coefficient of the PET port, respectively, and are both binary numbers with a value of 0 or 1. Table 3 presents the corresponding η_p and η_Q values of various control modes of the PET. Consequently, the number of independent control equations (Table 2) have been reduced to be further used in the unified representation of the power flow equations.

Table 3 The operating mode of the PET

Mode	Active power control	Reactive power control	η_p	η_Q	
AC port	s1	P_{ack}^H constant	Q_{ack}^H constant	1	1
	s2	/	U_{ack}^H constant	/	0
	s3	/	Q_{ack}^H constant	/	1
	s4	P_{ack}^H constant	U_{ack}^H constant	1	0
DC port	d1	U_{dck}^H constant	/	0	1
	d2	P_{dck}^H constant	/	1	1
	d3	$P_{dck}^H - U_{dck}^H$ Sag	/	0	0

4 Mixed power flow algorithms for multi-port PETs

4.1 Power flow equation of the AC–DC hybrid system with multi-port PETs

$$f(x_{hyb}) = f \begin{bmatrix} \theta_{aci} \\ U_{aci} \\ \theta'_{ack} \\ U'_{aci} \\ U_{dci} \\ U'_{dck} \end{bmatrix} = \begin{bmatrix} \Delta P_{aci} \\ \Delta Q_{aci} \\ \Delta P'_{ack} \\ \Delta Q'_{aci} \\ \Delta P_{dci} \\ \Delta P'_{dck} \end{bmatrix} \quad (17)$$

The power flow equation of the AC–DC hybrid system with the PET can be expressed by equation (17), where U_{aci} and θ_{aci} represent the voltage amplitude and phase

angle of the AC node, respectively; U'_{aci} and θ'_{ack} denote the voltage amplitude and phase angle of the AC contact node, respectively; U_{dci} is the DC voltage of the AC node; and U_{ack}^H represents the DC voltage of the DC connection node.

As observed in equation (17), the power flow calculation of the AC–DC hybrid system with the PET includes the following equations:

- 1) DC network power flow equation $\Delta P_{ack}^{loss}(U_{dci}, Y_{dc})$
- 2) AC system power flow equation $\Delta P_{aci}(\theta_{aci}, U_{aci})$
- 3) AC port power balance equation of AC–DC converter $\Delta P'_{ack}(\theta'_{ack}, U'_{ack})$, $\Delta Q'_{ack}(\theta'_{ack}, U'_{ack})$, and
- 4) DC port power balance equation of AC–DC converter $\Delta P'_{dck}(\theta'_{dck}, U'_{dck})$.

Under steady-state conditions, the power distribution of the DC network is expressed as follows:

$$\Delta P_{dci} = P_{dci} - \rho U_{dci} I_{dci} \quad (18)$$

Here, ρ represents the number of electrodes in the DC system. The current I_{dci} injected at the DC node i can be written as the sum of currents flowing to other (n-1) nodes in the network.

$$I_{dci} = \sum_{\substack{j=1 \\ j \neq i}}^n Y_{dcij} \cdot (U_{dci} - U_{dcj}) \quad (19)$$

To simplify the power flow equation, we rewrite equation (19) as a form of direct multiplication of the DC node admittance matrix and the DC node voltage.

$$I_{dci} = Y_{dc} U_{dc} \quad (20)$$

The DC current vector I_{dc} is expressed as $I_{dc} = [I_{dc1}, I_{dc2}, \dots, I_{dck}, 0, \dots, 0]^T$. As several inverters shut down or a few DC nodes are not connected to the AC system, the value of $n-k$ elements in I_{dc} is 0. The DC voltage vector U_{dc} can be expressed as $U_{dc} = [U_{dc1}, U_{dc2}, \dots, U_{dcn}]^T$. Y_{dc} is the DC node admittance matrix and can be expressed as equation (21).

$$Y_{dc} = \begin{bmatrix} y_{dl} & -y_{dl} \\ -y_{dl} & y_{dl} \end{bmatrix} \quad (21)$$

where y_{dl} is the series admittance value of the DC line connected to each DC node.

It should be highlighted that DC transformers are present in the complex DC system, and photovoltaic and DC energy storage are also connected to the DC system through the DC–DC converter. Therefore, when the DC network includes the DC–DC process, the DC node admittance matrix should be modified accordingly.

$$Y_{dc} = \begin{bmatrix} y_{DT} & -ky_{DT} \\ -ky_{DT} & k^2 y_{DT} \end{bmatrix} \quad (22)$$

Here, y_{DT} represents the internal impedance of the DC transformer and k represents the transformation ratio of the primary and secondary voltages of the DC transformer.

4.2 Iterative method based on step size optimization for the AC–DC mixed power flow

Typical AC–DC mixed power flow is generally solved using the alternating iteration method or the unified iterative method. However, AC–DC mixed power flow equations with multi-port PETs are much more complex than conventional AC–DC mixed power flow equations. The alternating iteration method cannot handle the return of the port equivalent power during the iteration process. The unified iteration method based on Newton's method has the problem of convergence caused by improper initial value selection owing to the addition of the PET control equation.

In this study, we improved the two power flow calculation methods to achieve AC and DC decoupling iterations while enhancing the convergence of the algorithm. To derive the algorithm, first we revised the power flow calculation equation (17).

$$\Delta f(x_{hyb}) = J \cdot \Delta x_{hyb} \quad (23)$$

Here, J represents the Jacobian matrix of the AC–DC mixed power flow equations. The Jacobian matrix can be express as equation (24).

$$\begin{bmatrix} \Delta P_{aci} \\ \Delta Q_{aci} \\ \Delta P'_{ack} \\ \Delta Q'_{ack} \\ \Delta P_{dci} \\ \Delta P'_{dck} \end{bmatrix} = - \begin{bmatrix} \frac{\partial \Delta P_{aci}}{\partial \theta_{aci}} & \frac{\partial \Delta P_{aci}}{\partial U_{aci}} & \frac{\partial \Delta P_{aci}}{\partial \theta'_{ack}} & \frac{\partial \Delta P_{aci}}{\partial U'_{ack}} & 0 & 0 \\ \frac{\partial \Delta Q_{aci}}{\partial \theta_{aci}} & \frac{\partial \Delta Q_{aci}}{\partial U_{aci}} & \frac{\partial \Delta Q_{aci}}{\partial \theta'_{ack}} & \frac{\partial \Delta Q_{aci}}{\partial U'_{ack}} & 0 & 0 \\ \frac{\partial \Delta P'_{ack}}{\partial \theta_{aci}} & \frac{\partial \Delta P'_{ack}}{\partial U_{aci}} & \frac{\partial \Delta P'_{ack}}{\partial \theta'_{ack}} & \frac{\partial \Delta P'_{ack}}{\partial U'_{ack}} & 0 & 0 \\ \frac{\partial \Delta Q'_{ack}}{\partial \theta_{aci}} & \frac{\partial \Delta Q'_{ack}}{\partial U_{aci}} & \frac{\partial \Delta Q'_{ack}}{\partial \theta'_{ack}} & \frac{\partial \Delta Q'_{ack}}{\partial U'_{ack}} & 0 & 0 \\ 0 & 0 & 0 & 0 & \frac{\partial \Delta P_{dci}}{\partial U_{dci}} & 0 \\ 0 & 0 & 0 & 0 & 0 & \frac{\partial \Delta P'_{dck}}{\partial U'_{dck}} \end{bmatrix} \begin{bmatrix} \Delta \theta_{aci} \\ \Delta U_{aci} \\ \Delta \theta'_{ack} \\ \Delta U'_{ack} \\ \Delta U_{dci} \\ \Delta U'_{dck} \end{bmatrix} \quad (24)$$

The Jacobian matrix can be express as equation (25).

$$J = \begin{bmatrix} J_{ac} & J_{ac}^{cov} & 0 \\ J_{ac}^{cov} & J_{cov} & 0 \\ 0 & 0 & J_{dc} \end{bmatrix} \quad (25)$$

Here, J_{ac} is the Jacobian matrix of the AC nodes, which represents the contribution of the AC node state to the node power correction. Further, J_{dc} is the DC system Jacobian matrix, which represents the contribution of the state quantity of the DC node (including DC contact nodes) to DC power corrections; J_{ac}^{cov} and J_{cov} are the AC–DC coupled Jacobian matrices, which represent the influence of the PET (or the VSC) port state quantity on the power correction amount of the port connection nodes and the AC nodes, respectively. In the actual power flow iteration process, the port state quantities of the PET and inverter are often specified by the control equation—that is, the port

state quantities are kept artificially set during the iteration process. Therefore, when the PET port is operating in constant power and constant voltage mode, the value of J_{ac}^{cov} is 0.

The unified iterative equation of the AC–DC mixed power flow correction equation is expressed as follows:

$$\begin{aligned} \Delta f^*(x_{hyb}^{(p+1)}) &= \Delta f(x_{hyb}^{(p)} + \Delta x_{hyb}^{(p)}) \\ &= \Delta f(x_{hyb}^{(p)}) + J^{(p)} \Delta x_{hyb}^{(p)} + H(\Delta x_{hyb}^{(p)}) \end{aligned} \quad (26)$$

where the state variable correction value $\Delta x_{hyb}^{(p)}$ includes the AC component $\Delta x_{ac}^{(p)}$ and the DC component $\Delta x_{dc}^{(p)}$, the superscript p indicates the number of current iterations, and n represents the sum of all higher-order terms. In the DC system,

$$H(\Delta x_{dc}^{(p)}) = \frac{1}{2} (x_{dc}^{(p)})^T [\nabla^2 f(x_{dc}^{(p)})] \Delta x_{dc}^{(p)} \quad (27)$$

In the AC system, the $H(\Delta x_{ac}^{(p)})$ value is 0. This difference leads to an asymmetry of the AC and DC iterative corrections. In the unified iteration process, when the initial value of the DC part is not selected appropriately, the AC power flow often diverges due to excessive corrections. To address this problem, we introduced the iteration step correction factor $\zeta^{(p)}$, and the iteration equation can be expressed as

$$\begin{aligned} \Delta f(x_{hyb}^{(p)} + \zeta^{(p)} \Delta x_{hyb}^{(p)}) &= \Delta f(x_{hyb}^{(p)}) + \\ &\zeta^{(p)} J^{(p)} \Delta x_{hyb}^{(p)} + H(\zeta^{(p)} \Delta x_{hyb}^{(p)}) \end{aligned} \quad (28)$$

After introducing the correction factor, the high-order terms of the iterative equation of AC system can be approximated by Taylor expansion for the AC component.

$$H(\zeta^{(p)} \Delta x_{ac}^{(p)}) \approx (\zeta^{(p)})^2 H(\Delta x_{ac}^{(p)}) \quad (29)$$

In the DC system, the higher-order term expression of the iterative equation introducing the correction factor can be expressed as

$$\begin{aligned} H(\zeta^{(p)} \Delta x_{dc}^{(p)}) &= \frac{1}{2} (\zeta^{(p)})^2 (\Delta x_{dc}^{(p)})^T [\nabla^2 f(x_{dc}^{(p)})] \Delta x_{dc}^{(p)} \\ &= (\zeta^{(p)})^2 H(\Delta x_{dc}^{(p)}) \end{aligned} \quad (30)$$

Therefore, the high-order term expressions of the AC–DC mixed power flow iteration equation can be uniformly expressed as

$$H(\zeta^{(p)} \Delta x_{hyb}^{(p)}) \approx (\zeta^{(p)})^2 H(\Delta x_{hyb}^{(p)}) = (\zeta^{(p)})^2 \Delta f(\Delta x_{hyb}^{(p+1)}) \quad (31)$$

Evidently, equation (29) only holds when the value of $\zeta^{(p)}$ tends to 0 or 1. The optimization model of the $\zeta^{(p)}$ value is expressed as follows:

$$\min F(\zeta^{(p)}) = \frac{1}{2} [\Delta f(x_{hyb}^{(p)} + \zeta^{(p)} \Delta x_{hyb}^{(p)})]^T \Delta f(x_{hyb}^{(p)} + \zeta^{(p)} \Delta x_{hyb}^{(p)}) \quad (32)$$

Let $\Delta f(x_{hyb}^{(p)}) = a^{(p)}$, $\Delta f(x_{hyb}^{(p)} + \Delta x_{hyb}^{(p)}) = b^{(p)}$; then, the constraints are expressed as follows:

$$h_3^{(p)} (\zeta^{(p)})^3 + h_2^{(p)} (\zeta^{(p)})^2 + h_1^{(p)} \zeta^{(p)} + h_0^{(p)} = 0 \quad (33)$$

$$\begin{cases} h_3^{(p)} = [b^{(p)}]^T b^{(p)} \\ h_2^{(p)} = -\frac{3}{2} [a^{(p)}]^T b^{(p)} \\ h_1^{(p)} = \frac{1}{2} [a^{(p)}]^T a^{(p)} + [a^{(p)}]^T b^{(p)} \\ h_0^{(p)} = -\frac{1}{2} [a^{(p)}]^T a^{(p)} \end{cases} \quad (34)$$

Fig. 3 shows the proposed algorithm flow chart.

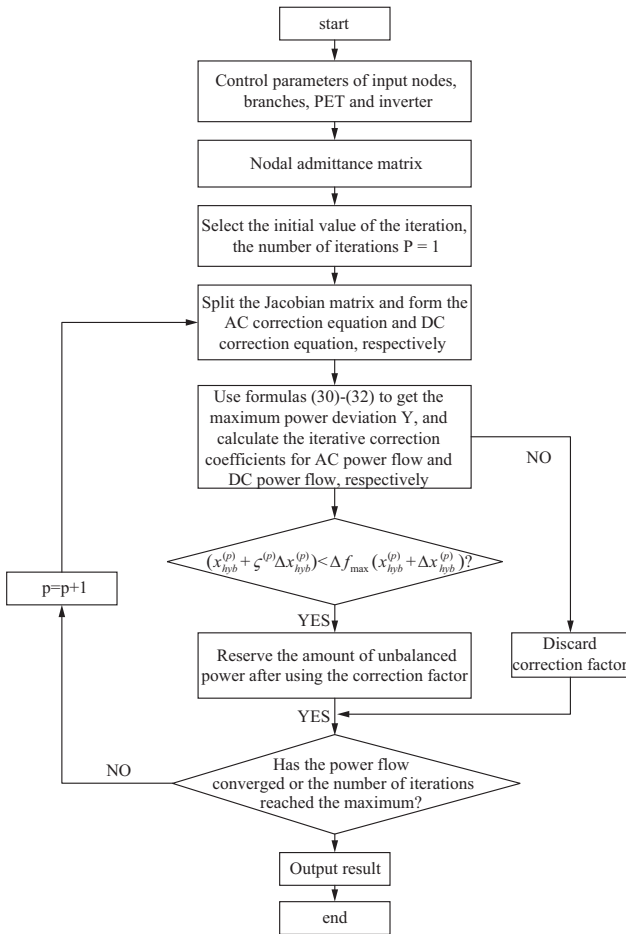


Fig. 3 Flow chart of the power flow calculation algorithm with the PET

To reduce the influence of the introduced step size correction factor on the iterative correction amount, the obtained maximum power difference between the AC node and the DC node at the $p+1$ iteration must be compared to obtain the maximum power difference, and the obtained maximum power difference should be compared also with the maximum power difference of the system obtained after introducing the iteration step correction factor. We used the smaller of the two sets of data as the state quantity

of the next iteration. The $x_{hyb}^{(p+1)}$ should satisfy the following equations.

$$x_{hyb}^{(p+1)} = \begin{cases} x_{hyb}^{(p)} + \Delta x_{hyb}^{(p)}, & \Delta f_{\max}^{(p)}(x_{hyb}^{(p)} + \zeta^{(p)} \Delta x_{hyb}^{(p)}) > \Delta f_{\max}^{(p)}(x_{hyb}^{(p)} + \Delta x_{hyb}^{(p)}) \\ x_{hyb}^{(p)} + \zeta^{(p)} \Delta x_{hyb}^{(p)}, & \Delta f_{\max}^{(p)}(x_{hyb}^{(p)} + \zeta^{(p)} \Delta x_{hyb}^{(p)}) < \Delta f_{\max}^{(p)}(x_{hyb}^{(p)} + \Delta x_{hyb}^{(p)}) \end{cases} \quad (35)$$

$$\Delta f_{\max}^{(p)}(x_{hyb}^{(p)} + \zeta^{(p)} \Delta x_{hyb}^{(p)}) = \max[\Delta f^{(p)}(x_{ac}^{(p)} + \zeta^{(p)} \Delta x_{ac}^{(p)}), \Delta f^{(p)}(x_{dc}^{(p)} + \zeta^{(p)} \Delta x_{dc}^{(p)})] \quad (36)$$

$$\Delta f_{\max}^{(p)}(x_{hyb}^{(p)} + \Delta x_{hyb}^{(p)}) = \max[\Delta f^{(p)}(x_{ac}^{(p)} + \Delta x_{ac}^{(p)}), \Delta f^{(p)}(x_{dc}^{(p)} + \Delta x_{dc}^{(p)})] \quad (37)$$

5 Case study

5.1 Test system

Based on the model and algorithm proposed in this study, we modified and re-programmed the equipment model and the main program of the basic function module provided by the open source software package MATA CDC and used the MATLAB platform to compile a multi-port PET AC-DC mixed power flow calculation program. The test system used in this study included multi-port PETs and multiple AC and DC voltage levels. Fig. 4 shows the test grid topology, and the details of the parameter data for the test system can be obtained from [30].

5.2 Calculation result analysis

To verify the effectiveness of the proposed algorithm, the proposed algorithm was compared with two traditional algorithms: 1) Algorithm 1, unified iteration method; 2) Algorithm 2, alternating iteration method; 3) Algorithm 3, iterative method based on simplified optimized Jacobian matrix and step size correction optimization proposed in this study. Table 4 present the basic parameters of the PET.

Table 4 The operating mode of the PET

	Port number	Connected node	Port impedance	Control mode and set value
PET1	H_1	D5	0.016+0.12j	s2: U_{ack}^H constant, 1.04
	L_1	C75	0.036	d1: U_{ack}^H constant, 0.6
	L_2	C88	0.022	d2: P_{ack}^H constant, 1.04
	L_3	D8	0.016+0.26j	s1: P_{ack}^H constant, 0.9; Q_{ack}^H constant, 0.3
PET2	H_1	D6	0.016+0.12j	s3: Q_{ack}^H constant, 0
	L_1	C44	0.039	d2: P_{ack}^H constant, 0.7
	L_2	C61	0.022	d1: U_{ack}^H constant, 1.04
	L_3	D7	0.016+0.26j	s1: P_{ack}^H constant, 0.8; Q_{ack}^H constant, 0.4

The maximum convergence accuracy of the three algorithms was set to 1×10^{-7} , and the initial value of the DC network voltage iteration was set to 1.04. Table 5 shows the calculation results and convergence iteration times of the three algorithms.

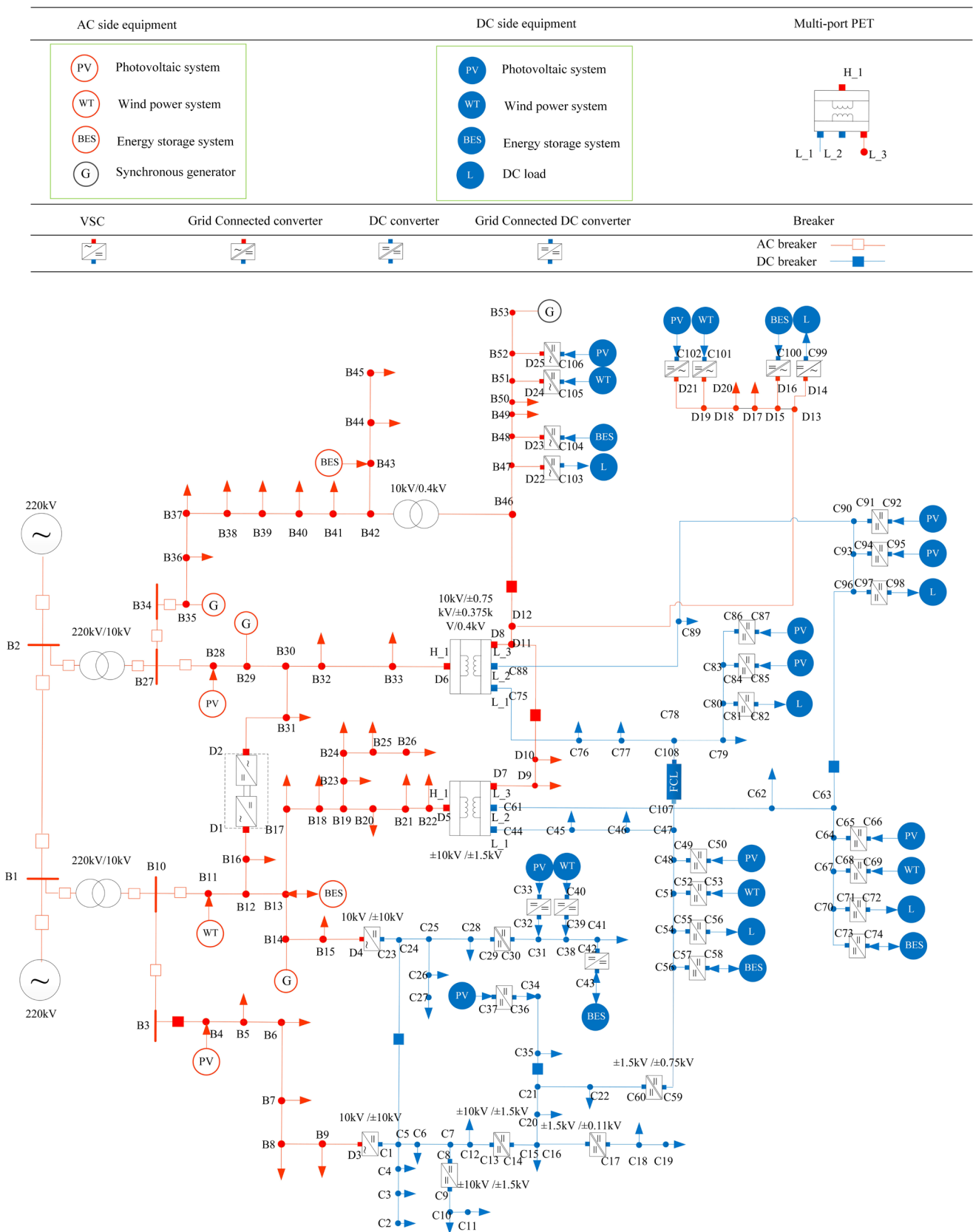


Fig. 4 Benchmark test system for the hybrid AC-DC distribution network with PETs

Table 5 The operating mode of the PET

Algorithm	Number of iterations	Maximum voltage deviation node	Maximum voltage deviation
1	34 AC iterations, 28 DC iterations	B19	0.90657
2	31	B30	0.08869
3	22	B46	0.05872

The calculation performance comparison presented in Table 5 indicates that only one iteration correction equation should be operated during the calculation process of Algorithm 2 unified iteration method. Further, the constraints of the power electronic transformer control equation are considered in the iterated Jacobian matrix;

hence, compared with the alternate iterative method of Algorithm 1 (which first makes the node equivalent and iterates the AC and DC iterative parts separately), Algorithm 2 has a faster convergence rate than Algorithm 1. Algorithm 3 adds the sparsity and symmetry of the Jacobian matrix on the basis of Algorithm 2, which further improves the convergence speed of Algorithm 3 over that of Algorithm 2. Moreover, under the condition that all three algorithms meet the convergence accuracy, the calculation deviation of Algorithm 3 is smaller. It should be noted that Algorithms 2 and 3 are both based on the basic principle of Newton's method, and a disadvantage of Newton's method is that it is more sensitive to the selection of initial values. To verify whether Algorithm 3 improves the sensitivity of the initial values, we compared the impact of different initial values on the calculation performance. Table 6 presents the comparison of the calculation results.

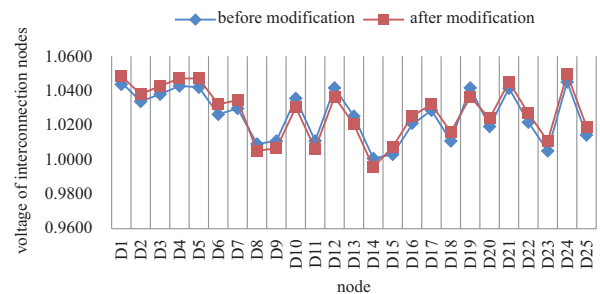
Table 6 Comparison of initial value sensitivity of different algorithms

Initial value of voltage	1.00	1.01	1.02	1.03	1.05	
Reached convergence?	No	Yes	Yes	Yes	Yes	
Algorithm 1	Number of iterations	/	AC36+DC29	AC30+DC26	AC29+DC25	AC28+DC26
	Maximum deviation	/	0.29869	0.25471	0.32862	0.37404
Reached convergence?	No	No	No	Yes	Yes	
Algorithm 2	Number of iterations	/	/	31	33	
	Maximum deviation	/	/	0.20789	0.33265	
Reached convergence?	No	Yes	Yes	Yes	Yes	
Algorithm 3	Number of iterations	/	28	26	23	25
	Maximum deviation	0.19879	0.17452	0.09578	0.12369	0.16238

From the comparison results in Table 6, we can observe that because Algorithm 3 optimizes the power flow iteration process, compared with Algorithm 2 (which does not limit the iteration process), Algorithm 3 exhibits a reduced sensitivity to the initial iteration value. This is because the iterative step size optimization technology proposed by Algorithm 3 effectively avoids the over-correction problem of Algorithm 2 during the iteration process. Considering that Algorithm 3 enhances the anti-interference ability of the unified iteration method and can also ensure better convergence accuracy, the algorithm proposed in this paper can be shown to have better computing performance and operational adaptability.

To verify the adaptability of the algorithm proposed in this study to different PET control modes, the control modes of the two PETs were adjusted as follows: the control mode of the low-voltage AC Port L₃ of PET1 was adjusted to

S4 mode, and the set value of the active power and voltage amplitude were adjusted to 0.8 and 1.03, respectively. The control mode of the low-voltage DC Port L₁ of PET2 was adjusted to d3, and the droop coefficient K was set to 0.75. After modifying the control mode, the algorithm proposed in this study still achieved convergence results. Fig. 5 shows


Fig. 5 Voltage comparison of interconnection nodes before and after modification of the PET control mode

the comparison of the interconnection node voltage before and after modification.

As shown in Fig. 5, after the control mode was modified, the voltage of the key interconnection node converged to the same value as before the modification, which verifies the accuracy of the PET model proposed in this paper.

6 Conclusion

In this study, based on the topology, power balance, loss, and control characteristics of multi-port PETs, we established a steady-state model of the PET and applied this state model to the power flow calculation of AC–DC hybrid systems with PETs. To address the new problems caused by the introduction of the PET port equations and control equations to the power flow calculation, we proposed an iterative method of AC–DC mixed power flow decoupling based on step optimization, which can achieve AC–DC decoupling and effectively improve convergence. The results demonstrate that the proposed algorithm improved the iterative method to overcome the over-correction and initial value sensitivity problems of conventional iterative algorithms.

Acknowledgements

This work was supported by the National Key Research and Development Program of China (2017YFB0903300).

References

- [1] J. Tian et al (2019) Individual DC Voltage Balance Control for Cascaded H-Bridge Electronic Power Transformer With Separated DC-Link Topology. *IEEE Access*, 7: 38558-38567
- [2] Q. Duan et al (2015) Flexible power distribution unit — A novel power electronic transformer development and demonstration for distribution system. *IECON 2015 - 41st Annual Conference of the IEEE Industrial Electronics Society*. Yokohama, 534-537
- [3] S. Shi, X. Wang and F. Zhong (2016) The research of typical control strategy of electronic power transformer in parallel operation. 2016 IEEE Advanced Information Management, Communicates, Electronic and Automation Control Conference (IMCEC), Xi'an, 1249-1252
- [4] G. Zhang, J. Chen, B. Zhang and Y. Zhang (2018) A critical topology review of power electronic transformers: In view of efficiency. *Chinese Journal of Electrical Engineering*, 4(2): 90-95
- [5] C. Gu, Z. Zheng, L. Xu, K. Wang and Y. Li (2016) Modeling and Control of a Multiport Power Electronic Transformer (PET) for Electric Traction Applications. *IEEE Transactions on Power Electronics*, 31(2): 915-927
- [6] X. Wang, J. Liu, S. Ouyang and F. Meng (2015) Research on Unbalanced-Load Correction Capability of Two Power Electronic Transformer Topologies. *IEEE Transactions on Power Electronics*, 30(6):3044-3056
- [7] A. -. Marten and D. Westermann (2012) A novel operation method for meshed HVDC overlay grids and corresponding steady state and dynamic power flow calculation principle. 10th IET International Conference on AC and DC Power Transmission (ACDC 2012), Birmingham, 1-6
- [8] J. Beerten, S. Cole and R. Belmans (2012) Generalized Steady-State VSC MTDC Model for Sequential AC/DC Power Flow Algorithms. *IEEE Transactions on Power Systems*, 27(2): 821-829
- [9] L. Xiao, Z. Xu, T. An and Z. Bian (2017) Improved Analytical Model for the Study of Steady State Performance of Droop-Controlled VSC-MTDC Systems. *IEEE Transactions on Power Systems*, 32(3): 2083-2093
- [10] D. Wang, C. Mao and J. Lu (2007) Modelling of electronic power transformer and its application to power system. *IET Generation, Transmission & Distribution*, 1(6): 887-895
- [11] A. A. Hamad, M. A. Azzouz and E. F. El Saadany (2016) A Sequential Power Flow Algorithm for Islanded Hybrid AC/DC Microgrids. *IEEE Transactions on Power Systems*, 31(5): 3961-3970
- [12] W. Wang and M. Barnes (2014) Power Flow Algorithms for Multi-Terminal VSC-HVDC With Droop Control. *IEEE Transactions on Power Systems*, 29(4): 1721-1730
- [13] E. Karami, G. B. Gharehpetian, H. Mohammadpour, A. Khalilinia and A. Bali (2020) Generalised representation of multi-terminal VSC-HVDC systems for AC–DC power flow studies. *IET Energy Systems Integration*, 2(1): 50-58
- [14] M. Baradar and M. Ghandhari (2013) A Multi-Option Unified Power Flow Approach for Hybrid AC/DC Grids Incorporating Multi-Terminal VSC-HVDC. *IEEE Transactions on Power Systems*, 28(3): 2376-2383
- [15] Mousavizadeh, Saeed, Haghifam, Mahmoudâ Reza (2016) A new approach for load flow calculation in AC/DC distribution networks considering the control strategies of different converters. *International Transactions on Electrical Energy Systems*, 26(11): 2479-2493
- [16] Huang, A. Q et al (2011) The Future Renewable Electric Energy Delivery and Management (FREEDM) System: The Energy Internet. *Proceedings of the IEEE*, 99(1) :133-148
- [17] Y. Yang, W. Pei, W. Deng and S. Zhang (2019) Benefit analysis of using multi-port and multi-function power electronic transformer connecting hybrid AC/DC power grids. *The Journal of Engineering*, 16: 1076-1080
- [18] M. Gao, K. Wang and L. He (2018) Probabilistic Model Checking and Scheduling Implementation of an Energy Router System in Energy Internet for Green Cities. *IEEE Transactions on Industrial Informatics*, 14(4): 1501-1510
- [19] L. Dong, T. Zhang, T. Pu, N. Chen and Y. Sun (2019) A Decentralized Optimal Operation of AC/DC Hybrid Microgrids Equipped With Power Electronic Transformer. *IEEE Access*, 7: 157946-157959
- [20] Zhang Bo, Tang Yu, Cong Pengwei et al (2017) Multi-time-scale

optimization control of AC-DC hybrid distribution network based on SOP and VSC. *New Technology of Electrical Engineering and Energy*, 9: 11-19

- [21] Miao J, Zhang N, Kang C et al (2017) Steady-state power flow model of energy router embedded AC network and its application in optimizing power system operation. *IEEE Transactions on Smart Grid*, 99: 1-1
- [22] Sun Chuangbo, Li Peng, Wang Chengshan et al (2015) Load flow calculation method for hybrid distribution active distribution network with multiple DC links. *Automation of Electric Power Systems*, 21: 59-65
- [23] S. Cole, J. Beerten and R. Belmans (2010) Generalized Dynamic VSC MTDC Model for Power System Stability Studies. *IEEE Transactions on Power Systems*, 25(3): 1655-1662
- [24] Xuan Wei, J. H. Chow, B. Fardanesh and A. -. Edris (2004) A common modeling framework of voltage-sourced converters for load flow, sensitivity, and dispatch analysis. *IEEE Transactions on Power Systems*, 19 (2): 934-941
- [25] L. Tang and B. Ooi (2007) Locating and Isolating DC Faults in Multi-Terminal DC Systems. *IEEE Transactions on Power Delivery*, 22(3): 1877-1884
- [26] Zhang Yantao, Qin Xiaohui, Zhou Qinyong et al (2015) Research on the method for obtaining feasible solutions of power flow calculation for hybrid power grids of large-scale AC/DC hybrid based on AC/DC decoupling. *Proceedings of the CSEE*, 24: 6275-6282
- [27] Baradar M, Hesamzadeh M R, Ghandhari M (2013) Second-order cone programming for optimal power flow in VSC-type AC-DC grids. *IEEE Transactions on Power Systems*, 4: 4282-4291
- [28] Xue S, Chen C, Yi J et al (2014) A research review of protection technology for DC distribution system. *Proceedings of the CSEE*, 34(19): 3114-3122
- [29] Kong Li, Yu Wei, Ye Hua et al (2017) Study on morphology, control and stability of AC/DC hybrid power distribution system. *New Technology of Electrical Engineering and Energy*, 9: 1-10
- [30] Cheng Lin, Tian Liting, Ge Xianjun et al (2019) A benchmark test system for multi-voltage hybrid ac/dc distribution network integrated with distribution resources. *Advanced Technology of Electrical Engineering and Energy*, 38(02): 60-71

Biographies



Hang Yin received his B.S. degree from Sichuan University, China, in 2018, and is a graduate student at Sichuan University. His research interests include power system planning and reliability assessment.



Qiang Li is now a senior engineer of the State Grid Jiangsu Electric Power Research Institute. His major research interests include new energy grid connection technology, energy storage, and comprehensive energy technology.



Youbo Liu received his Ph.D. from Sichuan University, China, in 2011, where he is currently an Associate Professor at the College of Electrical Engineering and Information Technology. His research interests include power system planning, power markets, and smart grids.



Xianglong Liu received his B.S. degree from Sichuan University, China, in 2017, and is a graduate student at Sichuan University. His research interests include power distribution network planning and renewable energy.



Yue Xiang currently works at the Department of Electrical Engineering, Sichuan University. Yue does research in power system planning and optimal operation, electric vehicles, power economics, integrated energy system, and machine learning.



Junyong Liu received a Ph.D. from Brunel University, U.K., in 1998. He is a Professor with the School of Electrical Engineering and Information, Sichuan University, China. His research interests include power system planning, operation, stability, and computer applications.

(Editor Zhou Zhou)